Supplementary Material:

3D magnetic induction maps of nanoscale materials revealed by electron holographic tomography

Daniel Wolf[1], Luis Alfredo Rodriguez[2,3,5], Armand Béché[4], Elsa Javon[4], Luis Serrano[2,3,5], Cesar Magen[2,3,8], Christophe Gatel[3,5], Axel Lubk[1], Hannes Lichte[1], Sara Bals[4], Gustaaf Van Tendeloo[4], Amalio Fernández-Pacheco[6], José M. De Teresa[2,3,7], Etienne Snoeck[3,5]

[1] Triebenberg Laboratory, Institute of Structural Physics, Technische Universität Dresden, 01062 Dresden (Germany)

[2] Laboratorio de Microscopías Avanzadas (LMA), Instituto de Nanociencia de Aragón (INA), Universidad de Zaragoza, 50018 Zaragoza, Spain

[3] Transpyrenean Associated Laboratory for Electron Microscopy (TALEM), CEMES INA, CNRS-Universidad de Zaragoza, Toulouse, France.

[4] EMAT, University of Antwerp, Groenenborgerlaan 171, 2020 Antwerp, Belgium

[5] CEMES-CNRS 29, rue Jeanne Marvig, B.P. 94347 F-31055, Toulouse Cedex, France.

[6] Thin Film Magnetism Group, Cavendish Laboratory, University of Cambridge, JJ Thomson Avenue, CB3 0HE, Cambridge UK

[7] Instituto de Ciencia de Materiales de Aragón (ICMA), Departamento de Física de la Materia Condensada, Universidad de Zaragoza-CSIC, Pedro Cerbuna 12, 5009 Zaragoza, Spain

[8] Fundación ARAID, 50018, Zaragoza, Spain

S1 Growth of a cobalt nanowire by FEBID

A detailed sketch of the sample can be found in Fig. S1. FEBID processes are basically chemical vapor deposition processes locally triggered by the action of a focused electron beam, in this case the field emission electron gun of the FEI dual beam Helios 600 FIB instrument. This local procedure can be theoretically performed on any substrate, independently of their shape and structure. In this work the substrates used for the growth are Cu nanorods (Fig. S1a) that match the TEM tomography holder model 2050, Fischione Instruments. Although they are ended in a tip, the highest position of the substrate it not always perfectly centered. Dual beam systems doesn't allow the tilting the substrate more than 60 degrees, impeding the determination of its exact apex. In order to prevent some other parts of the substrate blocking the nanowire during the image recording process, we proceed sharpening of the tip using focused ion milling (Fig. S1a). Low doses of irradiation modify substantially the magnetic properties of cobalt deposits growth by FEBID [**1**,**2**]. Taking that into account, all the milling processes were performed prior to the deposition of the cobalt.

The cobalt deposition was performed using $Co_2(CO)_8$ as gas precursor. During a FEBID process, the secondary electrons generated by the electron beam will locally decompose gas precursor molecules adsorbed on a substrate into volatile and non-volatile elements. In this way, it is possible to pattern functional nanostructures in one single step. The main drawback of this technique is in general the low metal purity of the generated deposits, since a complete decomposition of the precursor molecules is rather difficult to achieve. However, by using $Co_2(CO)_8$ as gas precursor

this problem can be largely overcome, creating high purity structures with a cobalt content over 90 % [3,4,5,6,7]. The gas injecting system was placed 100 µm above the sample and 150 µm away from the center of the scanning area. The base pressure of the chamber was $6.88 \cdot 10^{-7}$ mbar and the pressure during the deposition was $3.90 \cdot 10^{-6}$ mbar. The beam parameters used were 3kV of accelerating voltage and 21 pA of beam current. The deposit was grown using just one pixel as a pattern during 1000 passes using a dwell time of 2 ms and a refresh time of 100 ms. The three dimensional nanowire deposited is 3 µm long and has a diameter of 100 nm in average at the time of the deposition. Exposure to atmosphere after the growth process could lead to oxidation of the pillar.

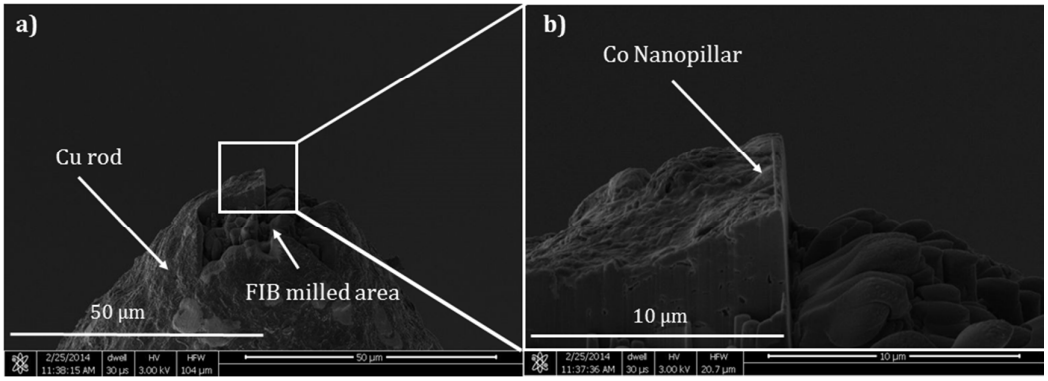

Figure S1: a) SEM image of the specimen under study. The copper rod used as a substrate and the FIB milled area highlighted. b) Zoom of the SEM image shown in a) centered on the cobalt NW grown by FEBID.

S2 STEM-EDX analysis

The composition of the nanowire was investigated by STEM EDX. A map of 108x464 pixels was acquired using a total time of 545 s. From the average spectrum analysis,

three atomic species were identified to be present in the sample: C, O and Co. The quantified analysis of the full map, based on a Cliff-Lorimer model with peak deconvolution, is displayed in Figure S2 a-d. One can clearly identify a core of Co-C and a shell of Co-O-C. The presence of carbon in the body of the nanowire is not surprising as the precursor used to grow the pillar by Focussed Electron Beam Induced Deposition (FEBID) is a carbon based gas. If part of the carbon is removed during the cracking process, it is always present in the final compound. Regarding the oxidized shell, its origin can be explained either by natural oxidation of the sample or by the plasma cleaning step carried out prior to insertion of the specimen in the TEM in order to reduce carbon contamination. A quantitative profile acquired across the pillar (Fig. S2 e) clearly shows the core shell structure. A profile calculated only from a geometrical point of view for a 59 nm core and an 8 nm shell radii was added to the figure and perfectly matches the oxygen profile. It is furthermore clear that the shell mainly corresponds to cobalt oxide as the C profile stops before the edges of the pillar.

In order to assess the average composition of the non-oxidized nanowire core, and thus the amount of cobalt participating to the global magnetization of the pillar, the quantitative analysis was calculated without the presence of oxygen. The resulting profile displayed in Fig. S2 f) reveal a content of 59.33 at% in Co and 40.66 at% in C.

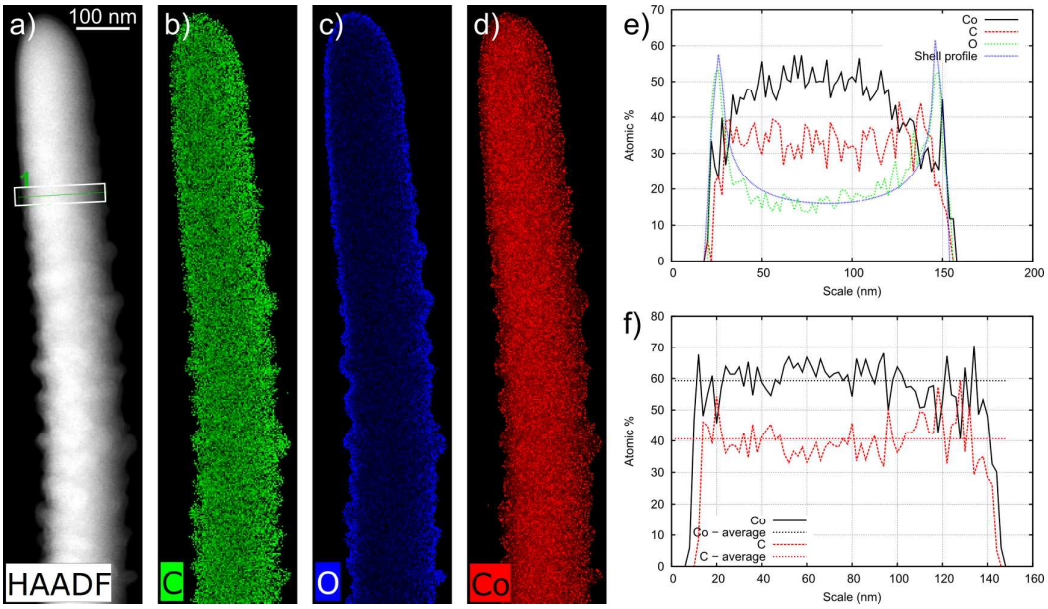

Figure S2: STEM-EDX analysis of the nanowire. a) STEM image of the nanowire together with b) the carbon map, c) the oxygen map and d) the cobalt map given as atomic %. e) Composition profile for the area marked as a white rectangle in a). A geometrically calculated shell profile was added to emphasize the O curve. f) Composition profile recalculated from e) without taken the O edge into account.

S3 Medium scale HAADF-STEM tomography

As the cobalt nanowire is not only composed of Co, we investigated its inner microstructure by conventional HAADF-STEM tomography. A single STEM image suggests that the pillar is composed of small filament, identified as cobalt according to their contrast, surrounded by a carbon matrix. In order to carefully investigate this growth mechanism, a 180° tilt series (2° step) of the pillar's tip was acquired and reconstructed using a SIRT algorithm (Fig. S3). From the orthoslice B obtained through the middle of the pillar, the cobalt filament seemed to have grown in a dendritic way. Orthoslice A, obtained closer to the surface, shows the filament structure even better since the shadowing effect is less present. This type of textured growth may have an influence on the final magnetization state of the pillar

and explain the lower magnetization value of the cobalt compared to the simulations.

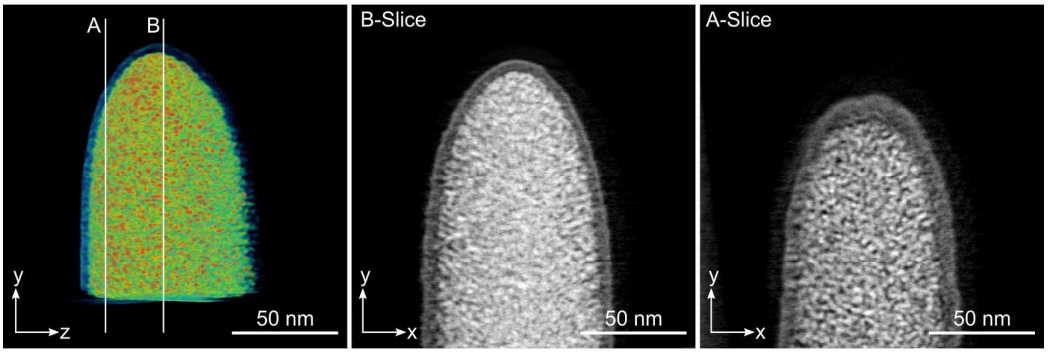

Figure S3: HAADF-STEM tomography reconstruction of the cobalt nanowire with two orthoslices (A) and (B) showing the cobalt nanostructure close to the surface and in the middle of the device.

S4 Perturbation of reference wave

To investigate how the reference wave is perturbed by long-ranging magnetic stray fields arising from the magnetic sample during the acquisition of the object hologram, we recorded two empty holograms at well-defined positions: The first empty hologram, which is routinely used within the holographic reconstruction step for correction of imaging artefacts in the object hologram, is acquired at that position, where the reference wave for the object hologram was. To identify that position, the method explained in [**8**] is applied. The second empty hologram is acquired at twice the distance between object and first empty hologram. Thus, by reconstructing the first empty hologram with the second one the phase distribution of the reference wave is obtained. Fig. S4 shows this procedure and the resulting reference phase image. The latter exhibits only a small gradient (see phase profile of Fig. S4)

$$m = \frac{\Delta\varphi}{\Delta x} = -1.96 \times 10^{-4} \frac{rad}{nm} \;\Rightarrow\; B_{\perp,proj} = \frac{\hbar}{e} \cdot \frac{\Delta\varphi}{\Delta x} = -0.13\, Tnm$$

which leads to a projected magnetic field of -0.13 Tnm. Compared to the projected stray field in the vicinity of the sample of ca. 10 Tnm this is very weak.

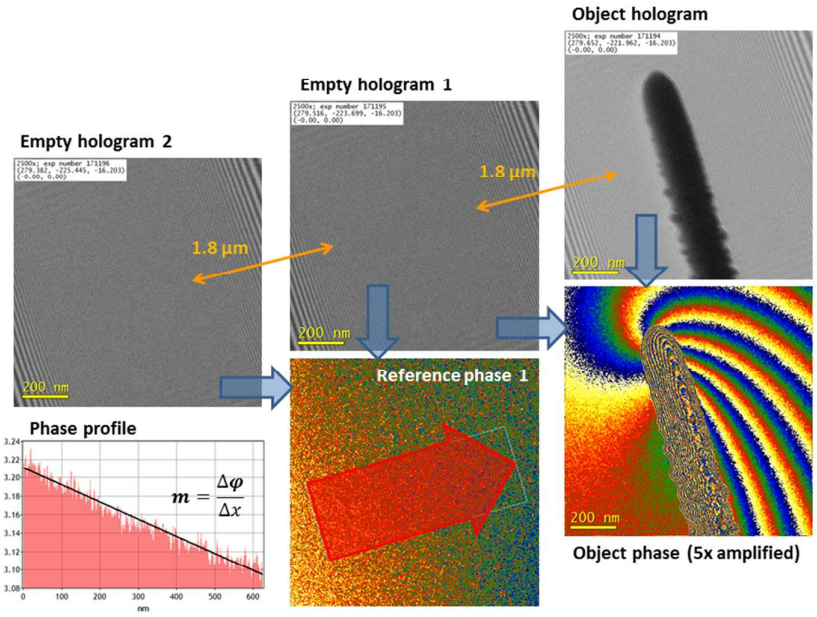

Figure S4: Examination of perturbed reference wave by reconstruction of its phase image. To this end, two empty holograms at well-defined positions are acquired and used for reconstruction of the reference phase. The latter exhibits only a small gradient as the phase profile supports.

S5 Stray field reconstruction

To complement our findings from the 3D reconstruction of the magnetic induction reported in the main text, we performed a dedicated reconstruction of the magnetic stray field around the nanowire only. Such a reconstruction uses only projection data from the exterior of the nanowire, which is sufficient for retrieving the exterior field (see Ref. [**9**] for details). It turns out that blocking the interior of the nanowire helps

to reduce artefacts from, e.g. misaligned tilt series, erroneous phase unwrapping, and dynamic scattering effects, because they predominantly occur within the nanowire but affect the reconstructed stray field due to the non-locality of the tomographic reconstruction in the standard reconstruction scheme (see again Ref. [**9**] for details). Fig. S5c exhibits the shape of the 3D magnetic stray field through a volume rendering of the reconstructed B_y component. It agrees very well with that of a homogeneously magnetized nanobar magnet, where the magnetic field is pushed out of the tip region (see Ref. [**9**] for magnetostatic simulations on a similar nanowire). This result confirms the monodomain structure only slightly perturbed by a small inversion domain in the tip region reported in the main text. We validate our findings by comparing the reprojected stray field from the tomographic reconstruction (Fig. S5d) with the experimental projections (Fig. S5b) obtained from the corresponding holographic phase image (Fig. S5a).

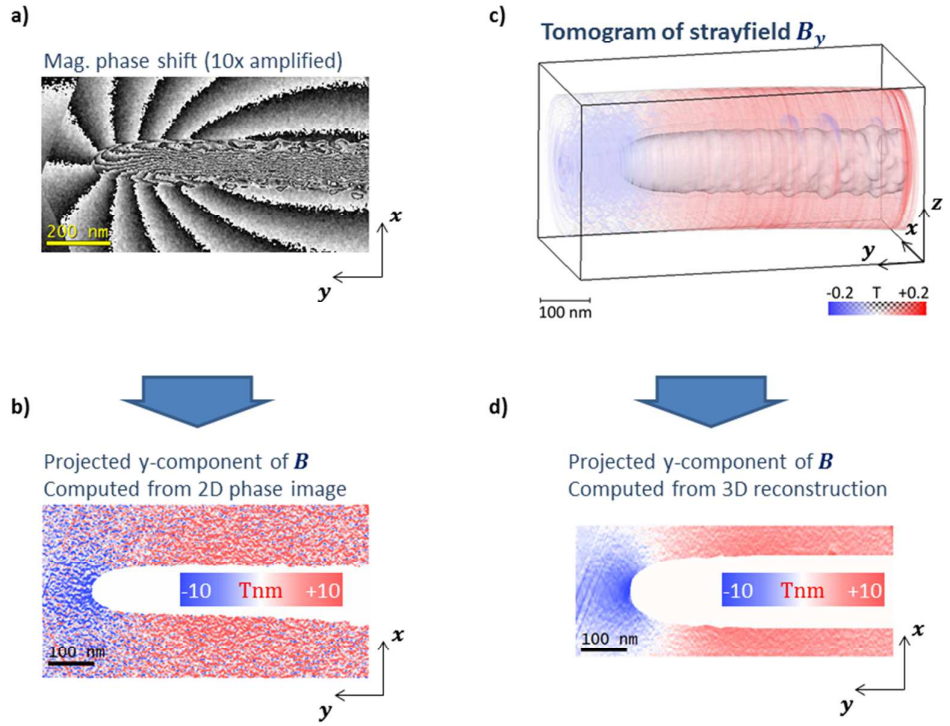

Figure S5: Magnetic stray fields around the Co NW. The isophase lines in one wrapped magnetic phase image (a) correspond to 2D field lines of the projected magnetic induction. The tilt series of projected magnetic stray fields (b) was used to reconstruct the 3D stray field depicted in (c). The characteristic shape of the 3D stray field resembling that of a nanobar magnet is confirmed by the re-projection (d) matching the original experimental data (b).

S6 Comparison between 3D reconstructions of potential and elastic attenuation

The so-called centerband intensity of an electron hologram visible as background of the fringe pattern corresponds to a conventional bright field TEM (BFTEM) image. In medium resolution it is formed by elastic scattering absorption contrast if using no energy filter. As recently demonstrated in [**10**], the tomographic reconstruction of the centerband intensity yields the 3D distribution of the elastic attenuation coefficient $\mu = n\sigma(\alpha)$, where n is the density of the atomic scatters, $\sigma(\alpha)$ their

elastic cross-section depending on the minimum aperture angle α for scattering absorption. It therefore provides information about the chemical composition (mass density). The latter is also provided by the reconstructed electric potential due to the MIP contribution. The electric potential can be however modulated additionally by purely electronic effects such as space charges. Figure 6 presents a comparison between the elastic attenuation reconstructed from centerband and the electric potential reconstructed from phase signal. Both reconstructions look rather similar, and thus the decrease of the potential towards the surface as clearly visible in the longitudinal section and the line profile can be explained mainly by a decrease of the mass density by comparison with the corresponding elastic attenuation data. However, the slight differences between both may occur from space charges modulating the potentials or residual phase contrast in the centerband images modulating the elastic attenuation tomogram, in particular at the object edges (higher spatial frequencies).

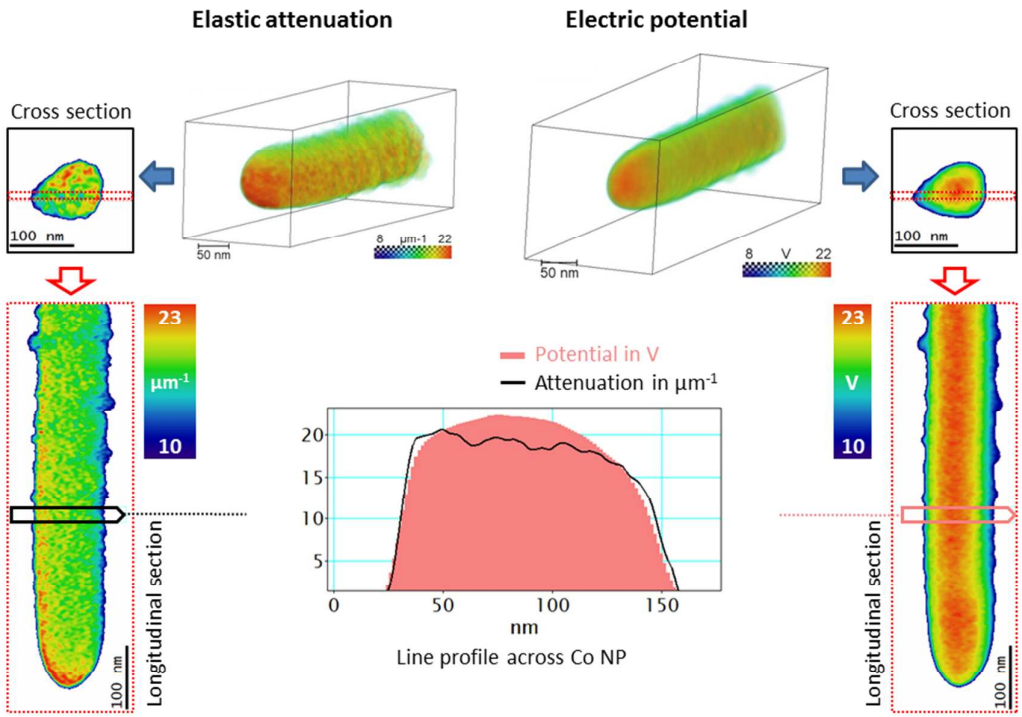

Figure S6: Elastic attenuation vs. electric potential of a Co nanowire reconstructed from a holographic tilt series.

S7 Lateral resolution

The lateral resolution is estimated on a representative cross-section of the Co NW's reconstructed 3D potential by analyzing the edge spread. Fig. S7 shows the cross-section with six line scans (1-6) along different directions from vacuum to the interior of the nanowire yielding the step function (blue filled). The derivative of the latter results in the edge spread function (ESF). As a measure of resolution, we use the full width half maximum (FWHM) of the peak in the ESF. For the six line profiles we obtain FWHM values between 7 nm and 10 nm.

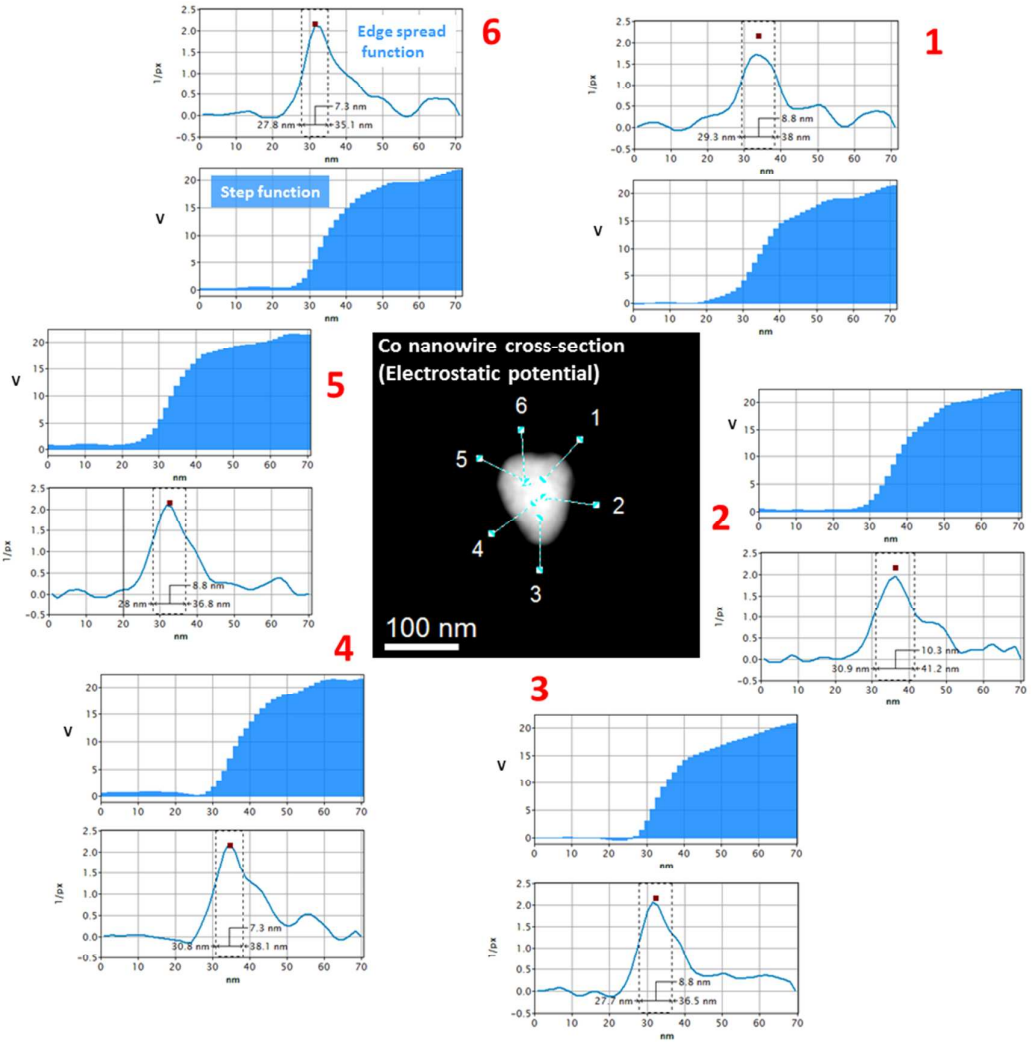

Figure S7: Determination of lateral resolution on a representative cross-section of the Co NW's reconstructed 3D potential. (1-6) Line scans and corresponding line profiles yielding the step function (blue filled), and its derivative, the edge spread function (blue line).

S8 Animations

Co-NW PhaseTiltSeries.mpg shows the reconstructed electric and magnetic phase shift from a hologram tilt series covering a tilt range of 180° in 3° steps. The electric

phase shift is visualized as greyscale (0-18 rad) and the magnetic as isolines (-3 rad to +3 rad in 1 rad steps).

Co-NW 3D Pot orthoslices.mpg and **Co-NW 3D By orthoslices.mpg** illustrate slices through the electric potential and longitudinal component of the magnetic induction normal the longitudinal (y) direction of the Co nanowire, respectively

Rotated 3D potential.mpg and **Rotated 3D B-field.mpg** animate the rotation electric potential and longitudinal component of the magnetic induction in volume and iso-surface representation. The 12 V iso-surface renders the 3D morphology of the NW and the 0.01 T iso-surface the 3D shape of the domain wall.

References

1 Serrano-Ramon, L., Fernandez-Pacheco, A., Cordoba, R. et al. Improvement of domain wall conduit properties in cobalt nanowires by global gallium irradiation. *Nanotechnology*, 24 (2013), 345703.

2 Serrano-Ramon, Luis, Fernandez-Pacheco, Amalio, Ibarra, Manuel Ricardo, Petit, Dorothée, Cowburn, Russell P., Tyliszczak, Tolek, and De Teresa, Jose Maria. Modification of domain-wall propagation in Co nanowires via Ga+ irradiation. *The European Physical Journal B*, 86 (2013), 97.

3 Utke, I., Michler, J., Gasser, Ph. et al. Cross Section Investigations of Compositions and Sub-Structures of Tips Obtained by Focused Electron Beam Induced Deposition. *Advanced Engineering Materials*, 7 (2005), 323.

4 Fernandez-Pacheco, A., De Teresa, J. M., Cordoba, R., and Ibarra, M. R. Magnetotransport properties of high-quality cobalt nanowires grown by focused-

electron-beam-induced deposition. *Journal of Physics D: Applied Physics*, 42 (2009), 055005.

5 Belova, L M, Dahlberg, E D, Riazanova, A, Mulders, J J L, Christophersen, C, and Eckert, J. Rapid electron beam assisted patterning of pure cobalt at elevated temperatures via seeded growth. *Nanotechnology*, 22 (2011), 145305--.

6 Serrano-Ramón, Luis, Córdoba, Rosa, Rodrigues, R. P.guez, Luis Alfredo et al. Ultrasmall Functional Ferromagnetic Nanostructures Grown by Focused Electron-Beam-Induced Deposition. *ACS Nano*, 5 (2011), 7781-7787.

7 Idigoras, O., Nikulina, E., Porro, J. M., Vavassori, P., Chuvilin, A., and Berger, A. FEBID fabrication and magnetic characterization of individual nano-scale and micro-scale Co structures. *Nanofabrication*, 1 (2014), 23-34.

8 Wolf, Daniel, Lubk, Axel, Lichte, Hannes, and Friedrich, Heiner. Towards automated electron holographic tomography for 3D mapping of electrostatic potentials. *Ultramicroscopy*, 110 (2010), 390-399.

9 Lubk, A., Wolf, D., Simon, P., Wang, C., Sturm, S., and Felser, C. Nanoscale three-dimensional reconstruction of electric and magnetic stray fields around nanowires. *Applied Physics Letters*, 105, 17 (2014), 173110.

10 Lubk, A., Wolf, D., Kern, F., Röder, F., Prete, P., Lovergine, N., and Lichte, H. Nanoscale three-dimensional reconstruction of elastic and inelastic mean free path lengths by electron holographic tomography. *Applied Physics Letters*, 105 (2014), 173101.